
USF Patents

June 2018

Electrodeposition of metal microstructures

Hesham Y. Saleh Mraied

Wenjun Cai

Follow this and additional works at: https://digitalcommons.usf.edu/usf_patents

Recommended Citation

Mraied, Hesham Y. Saleh and Cai, Wenjun, "Electrodeposition of metal microstructures" (2018). *USF Patents*. 1047.

https://digitalcommons.usf.edu/usf_patents/1047

This Article is brought to you for free and open access by Digital Commons @ University of South Florida. It has been accepted for inclusion in USF Patents by an authorized administrator of Digital Commons @ University of South Florida. For more information, please contact digitalcommons@usf.edu.



US010006134B1

(12) **United States Patent**
Mraied et al.

(10) **Patent No.:** **US 10,006,134 B1**
(45) **Date of Patent:** **Jun. 26, 2018**

(54) **ELECTRODEPOSITION OF METAL
MICROSTRUCTURES**

2008/0090108 A1* 4/2008 Uchida C25D 7/12
429/457
2014/0170303 A1* 6/2014 Rayner C25D 1/00
427/58

(71) Applicants: **Hesham Y. Saleh Mraied**, Tampa, FL
(US); **Wenjun Cai**, Tampa, FL (US)

(72) Inventors: **Hesham Y. Saleh Mraied**, Tampa, FL
(US); **Wenjun Cai**, Tampa, FL (US)

(73) Assignee: **University of South Florida**, Tampa,
FL (US)

(*) Notice: Subject to any disclaimer, the term of this
patent is extended or adjusted under 35
U.S.C. 154(b) by 214 days.

(21) Appl. No.: **14/935,398**

(22) Filed: **Nov. 7, 2015**

Related U.S. Application Data

(60) Provisional application No. 62/076,591, filed on Nov.
7, 2014.

(51) **Int. Cl.**
C25D 1/00 (2006.01)
B32B 15/01 (2006.01)
C25D 3/56 (2006.01)
C25D 1/02 (2006.01)

(52) **U.S. Cl.**
CPC **C25D 1/003** (2013.01); **B32B 15/016**
(2013.01); **C25D 1/02** (2013.01); **C25D 3/56**
(2013.01)

(58) **Field of Classification Search**
None
See application file for complete search history.

(56) **References Cited**

U.S. PATENT DOCUMENTS

3,663,404 A * 5/1972 Loop B01D 61/025
204/482

OTHER PUBLICATIONS

Fleck, N.A., V.S. Deshpande, and M.F. Ashby, Micro-architected
materials: past, present and future. P Roy Soc a-Math Phy, 2010.
466(2121): p. 2495-2516.

Kolodziejska, J.A., C.S. Roper, S.S. Yang, W.B. Carter, and A.J.
Jacobsen, Research Update: Enabling ultra-thin lightweight struc-
tures: Microsandwich structures with microlattice cores. Apl Mater,
2015. 3(5).

Xiong, J., R. Mines, R. Ghosh, A. Vaziri, L. Ma, A. Ohrndorf, H.
Christ, and L. Wu, Advanced Micro-Lattice Materials. Advanced
Engineering Materials, 2015: p. 1-12.

Tian, J., T. Kim, T.J. Lu, H.P. Hodson, D.T. Queheillalt, D.J. Sypeck,
and H.N.G. Wadley, The effects of topology upon fluid-flow and
heat-transfer within cellular copper structures. Int J Heat Mass Tran,
2004. 47(14-16): p. 3171-3186.

Lu, T.J., L. Valdevit, and A.G. Evans, Active cooling by metallic
sandwich structures with periodic cores. Prog Mater Sci, 2005.
50(7): p. 789-815.

(Continued)

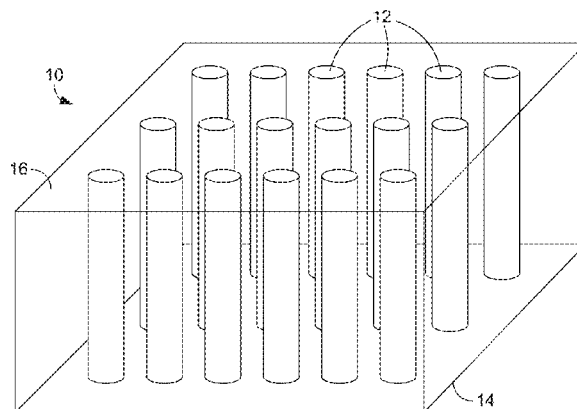
Primary Examiner — John J Figueroa

(74) *Attorney, Agent, or Firm* — Thomas I Horstemeyer,
LLP

(57) **ABSTRACT**

In one embodiment, a method for fabricating a metal micro-
structure includes forming a non-conductive polymer mem-
brane having a plurality of pores, coating at least one end of
the membrane and inner surfaces of the pores with a
conductive material to form a conductive coating, electrode-
positing a metal on the conductive coating, and dissolving
the membrane to obtain a free-standing metal microstructure
having at least one metal end plate and multiple elongated
metal members extending therefrom.

15 Claims, 9 Drawing Sheets



(56)

References Cited

OTHER PUBLICATIONS

- Roper, C.S., Multiobjective optimization for design of multifunctional sandwich panel heat pipes with micro-architected truss cores. *Int J Heat Fluid Fl*, 2011. 32(1): p. 239-248.
- Gu, et al., "Ultra-strong architected Cu meso-lattices", *Extreme Mechanics letters*; ScienceDirect 2, 2015.
- McCormack, T.M., R. Miller, O. Kesler, and L.J. Gibson, Failure of sandwich beams with metallic foam cores. *Int J Solids Struct*, 2001. 38(28-29): p. 4901-4920.
- Shen, Y., S. McKown, S. Tsopanos, C.J. Sutcliffe, R.A.W. Mines, and W.J. Cantwell, The Mechanical Properties of Sandwich Structures Based on Metal Lattice Architectures. *J Sandw Struct Mater*, 2010. 12(2): p. 159-180.
- Wadley, H.N.G., N.A. Fleck, and A.G. Evans, Fabrication and structural performance of periodic cellular metal sandwich structures. *Compos Sci Technol*, 2003. 63(16): p. 2331-2343.
- Yin, S., L.Z. Wu, L. Ma, and S. Nutt, Hybrid truss concepts for carbon fiber composite pyramidal lattice structures. *Compos Part B-Eng*, 2012. 43(4): p. 1749-1755.
- Meza, L.R., S. Das, and J.R. Greer, Strong, lightweight, and recoverable three-dimensional ceramic nanolattices. *Science*, 2014. 345(6202): p. 1322-1326.
- Ruan, S.Y. and C.A. Schuh, Electrodeposited Al—Mn alloys with microcrystalline, nanocrystalline, amorphous and nano-quasicrystalline structures. *Acta Mater*, 2009. 57(13): p. 3810-3822.
- Ruan, S.Y. and C.A. Schuh, Towards electroformed nanostructured aluminum alloys with high strength and ductility. *J Mater Res*, 2012. 27(12): p. 1638-1651.
- Olson, J., A. Manjavacas, L. Liu, W. Chang, B. Foerster, N.S. King, M.W. Knight, P. Nordlander, N.J. Halas, and S. Link, Vivid, full-color aluminum plasmonic pixels. *P Natl Acad Sci USA*, 2014. 111(40): p. 14348-14353.
- Cheah, S.K., E. Perre, M. Rooth, M. Fondell, A. Harsta, L. Nyholm, M. Boman, T. Gustafsson, J. Lu, P. Simon, and K. Edstrom, Self-Supported Three-Dimensional Nanoelectrodes for Microbattery Applications. *Nano Lett*, 2009. 9(9): p. 3230-3233.
- Oltean, G., L. Nyholm, and K. Edstrom, Galvanostatic electrodeposition of aluminium nano-rods for Li-ion three-dimensional micro-battery current collectors. *Electrochim Acta*, 2011. 56(9): p. 3203-3208.
- Deshpande, V.S. and N.A. Fleck, High strain rate compressive behaviour of aluminium alloy foams. *Int J Impact Eng*, 2000. 24(3): p. 277-298.
- Mukai, T., H. Kanahashi, T. Miyoshi, M. Mabuchi, T.G. Nieh, and K. Higashi, Experimental study of energy absorption in a close-celled aluminum foam under dynamic loading. *Scripta Mater*, 1999. 40(8): p. 921-927.
- Verdieck, R.G. and L.F. Yntema, The electrochemistry of baths of fused aluminum halides I Aluminum as a reference electrode. *J Phys Chem-U.S.*, 1942.46(3): p. 344-352.
- Tsuda, T., C.L. Hussey, and G.R. Stafford, Electrodeposition of Al—Mo—Mn ternary alloys from the Lewis acidic AlCl₃-EtMelmCl molten salt. *J Electrochem Soc*, 2005. 152(9): p. C620-C625.
- Su, C.J., Y.T. Hsieh, C.C. Chen, and I.W. Sun, Electrodeposition of aluminum wires from the Lewis acidic AlCl₃/trimethylamine hydrochloride ionic liquid without using a template. *Electrochem Commun*, 2013. 34: p. 170-173.
- Uchida, J., T. Tsuda, Y. Yamamoto, H. Seto, M. Abe, and A. Shibuya, Electroplating of Amorphous Aluminum Manganese Alloy from Molten-Salts. *Isij Int*, 1993. 33(9): p. 1029-1036.
- Stafford, G.R. and C.L. Hussey, Electrodeposition of Transition Metal-Aluminum Alloys from Chloroaluminate Molten Salts, in *Advances in Electrochemical Science and Engineering*. 2001, Wiley-VCH Verlag GmbH: Weinheim. p. 313-328.
- Boon, J.A., J.A. Levisky, J.L. Pflug, and J.S. Wilkes, Friedel Crafts Reactions in Ambient-Temperature Molten-Salts. *J Org Chem*, 1986. 51(4): p. 480-483.
- Li, Q.F., H.A. Hjuler, R.W. Berg, and N.J. Bjerrum, Electrochemical Deposition and Dissolution of Aluminum in NaAlCl₄ Melts—Influence of MnCl₂ and Sulfide Addition. *J Electrochem Soc*, 1990. 137(9): p. 2794-2798.
- Huo, S. and W. Schwarzscher, Anomalous scaling of the surface width during Cu electrodeposition. *Phys Rev Lett*, 2001. 86(2): p. 256-259.
- Dammers, A.J. and S. Radelaar, 2-Dimensional Computer Modeling of Polycrystalline Film Growth. *Texture Microstrud*, 1991. 14: p. 757-762.
- Liu, X.J., I. Ohnuma, R. Kainuma, and K. Ishida, Thermodynamic assessment of the aluminum-manganese (Al—Mn) binary phase diagram. *J Phase Equilib*, 1999. 20(1): p. 45-56.
- Tian, M.L., J.U. Wang, J. Kurtz, T.E. Mallouk, and M.H.W. Chan, Electrochemical growth of single-crystal metal nanowires via a two-dimensional nucleation and growth mechanism. *Nano Lett*, 2003. 3(7): p. 919-923.
- Oliver, W.C. and G.M. Pharr, An improved technique for determining hardness and elastic modulus using load and displacement sensing indentation experiments. *Journal of Materials Research*, 1992. 7(06): p. 1564-1583.
- Kolodziejska, et al., "Research Update: Enabling ultra-thin lightweight structures: Microsandwich structures with microlattice cores", AIP Materials. AIP Publishing, 2015.
- Shuaieb, F.M. and P.D. Soden, Indentation failure of composite sandwich beams. *Compos Sci Technol*, 1997. 57(9-10): p. 1249-1259.
- Lewandowski, J.J., W.H. Wang, and A.L. Greer, Intrinsic plasticity or brittleness of metallic glasses. *Phil Mag Lett*, 2005. 85(2): p. 77-87.

* cited by examiner

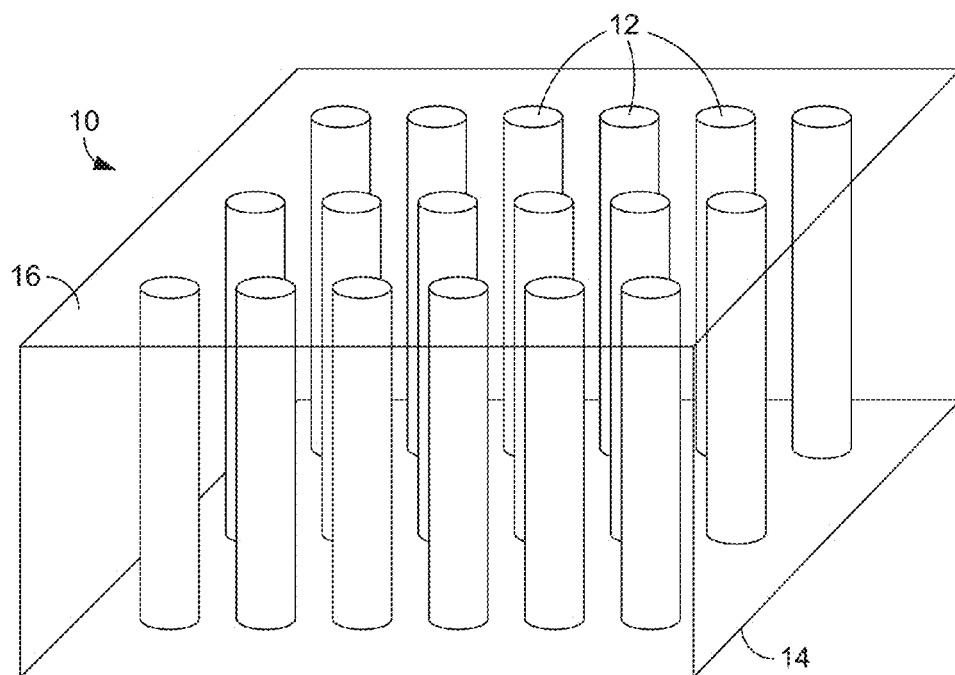


FIG. 1A

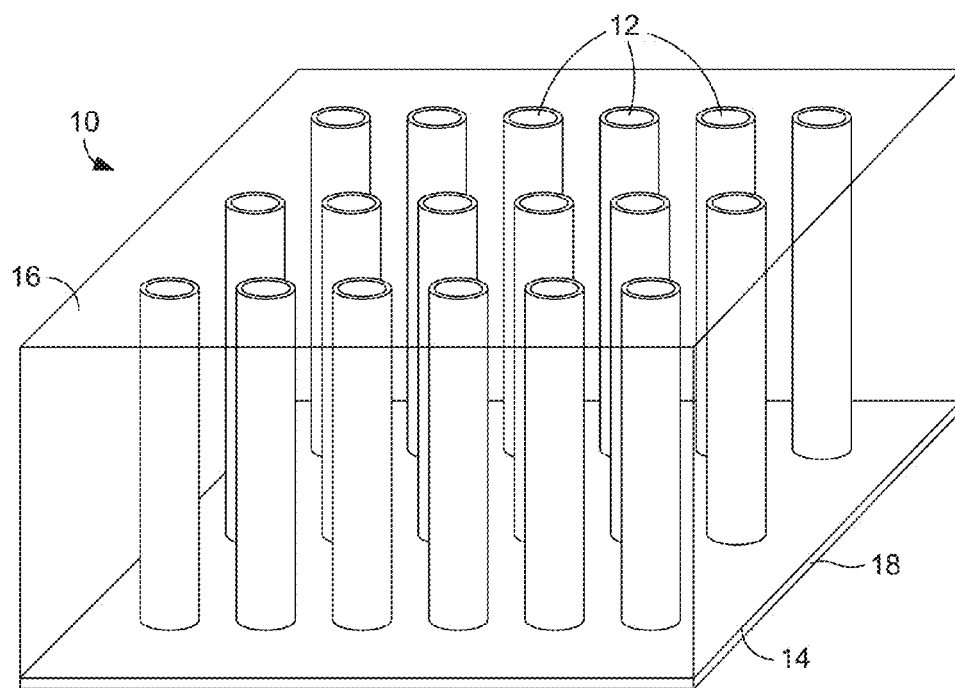


FIG. 1B

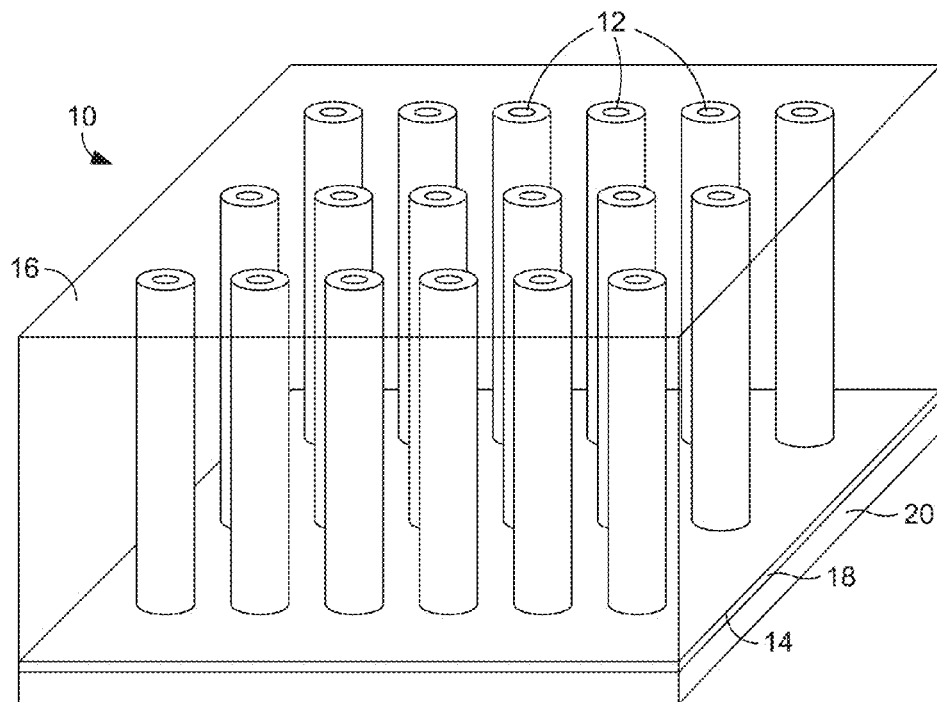


FIG. 1C

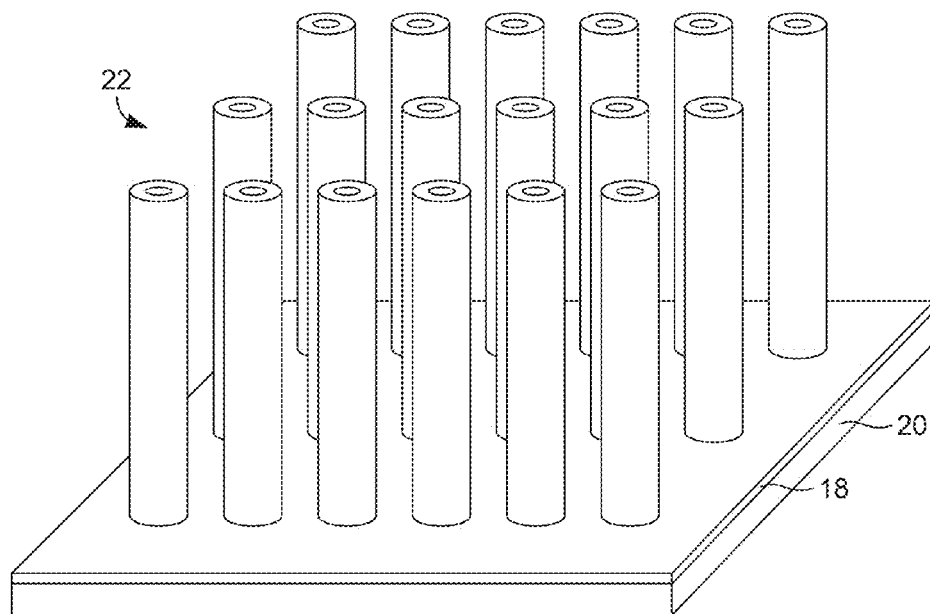


FIG. 1D

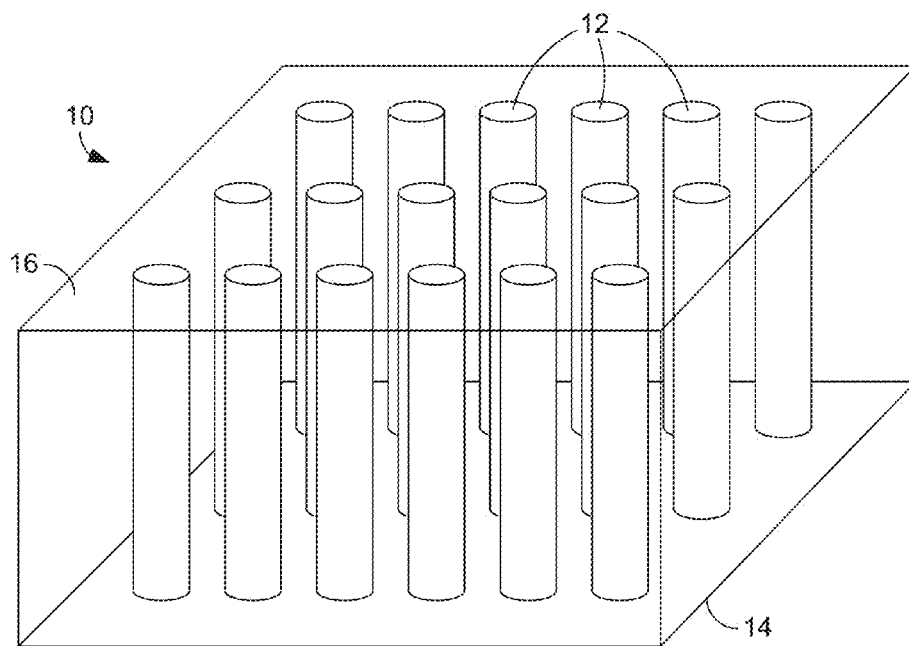


FIG. 2A

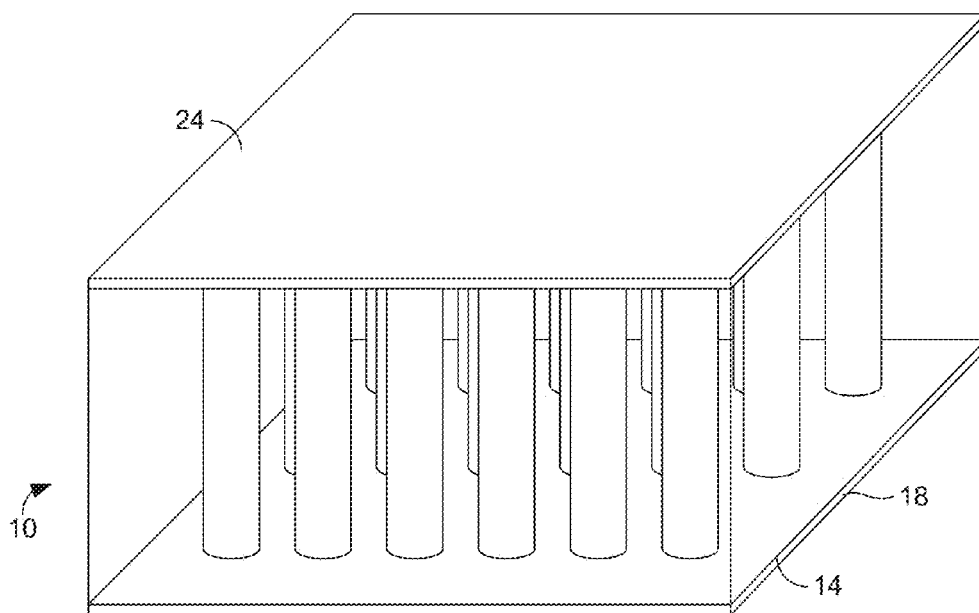


FIG. 2B

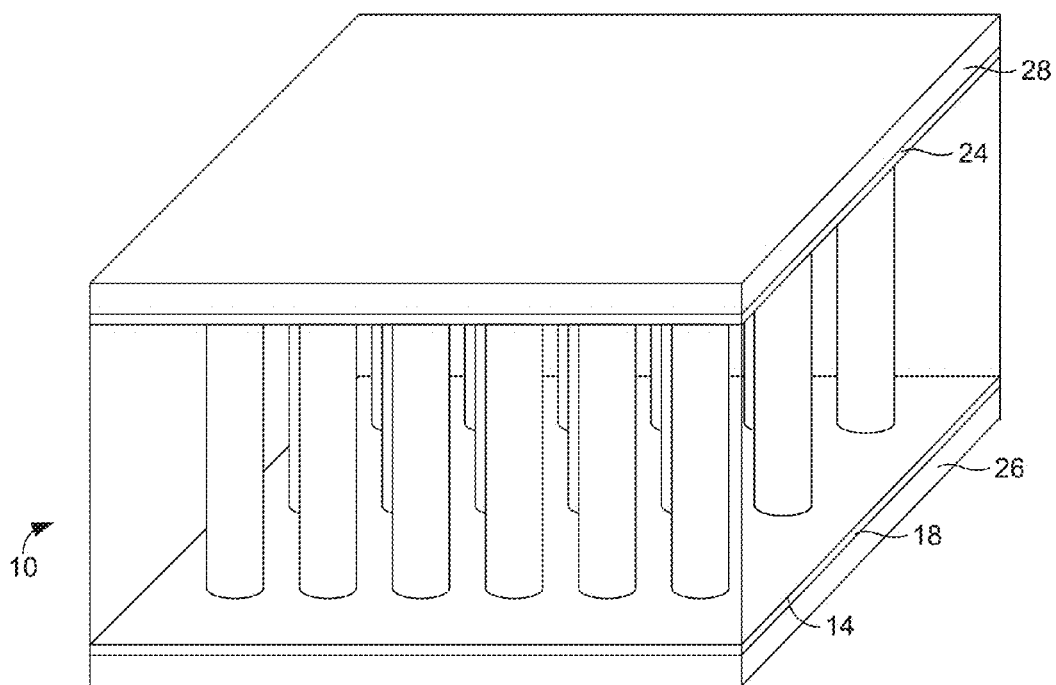


FIG. 2C

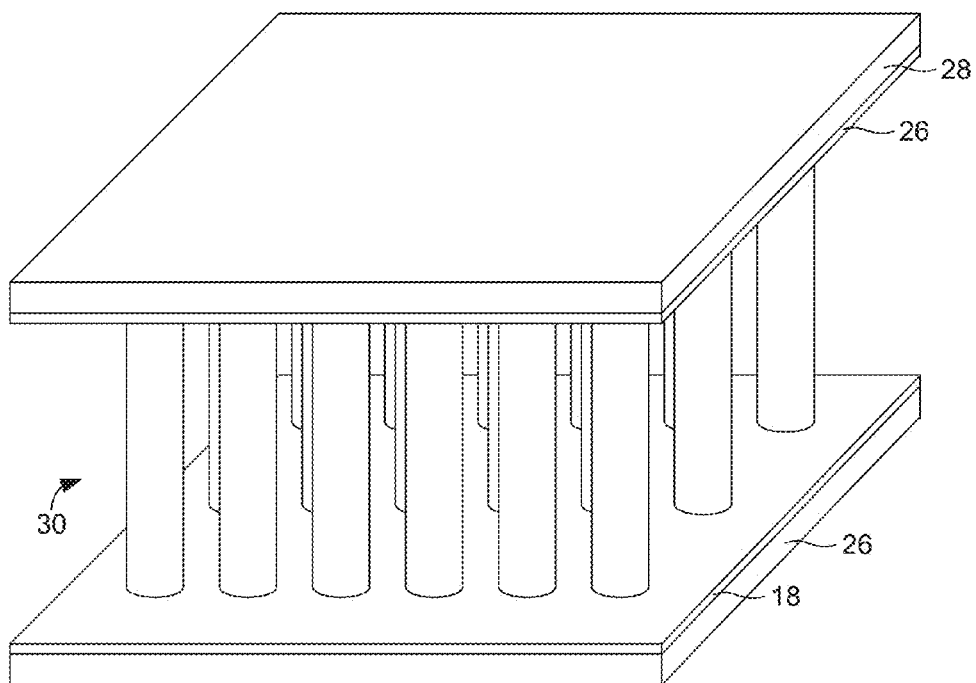
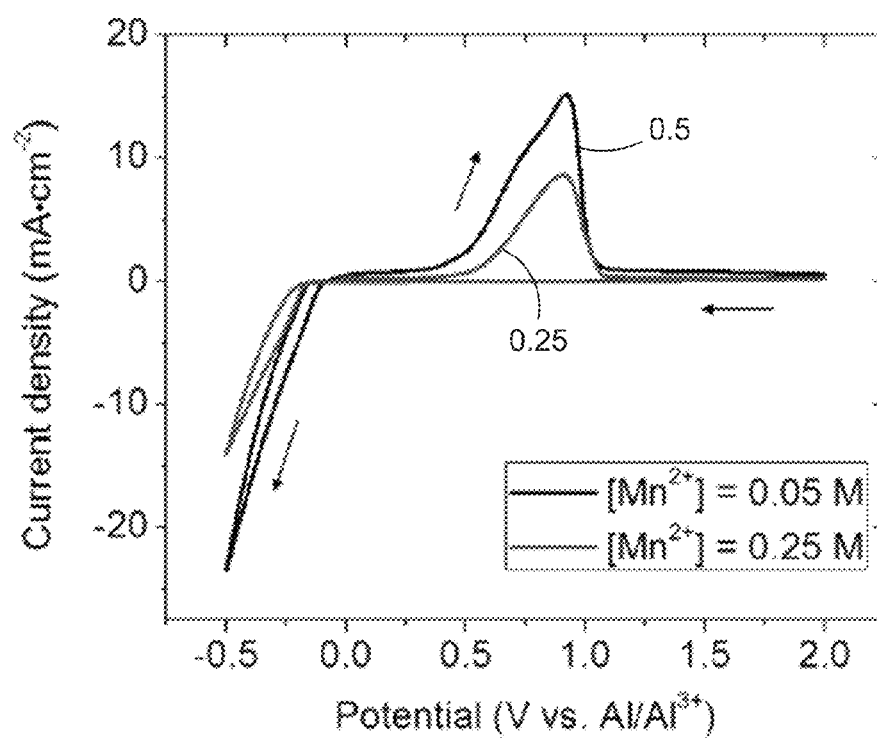


FIG. 2D

**FIG. 3**

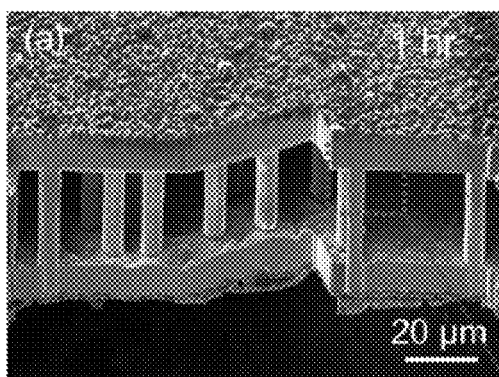


FIG. 4A

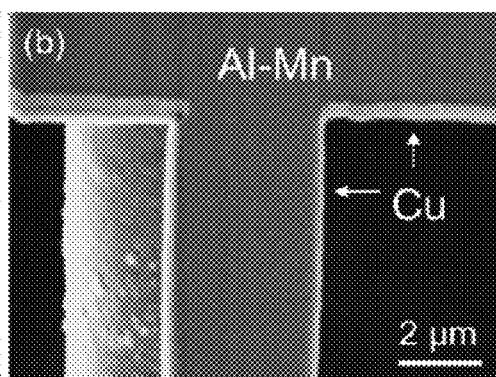


FIG. 4B

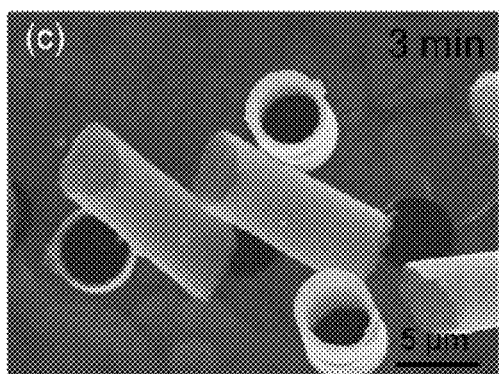


FIG. 4C

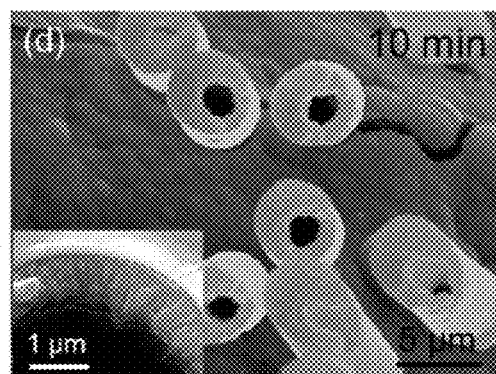
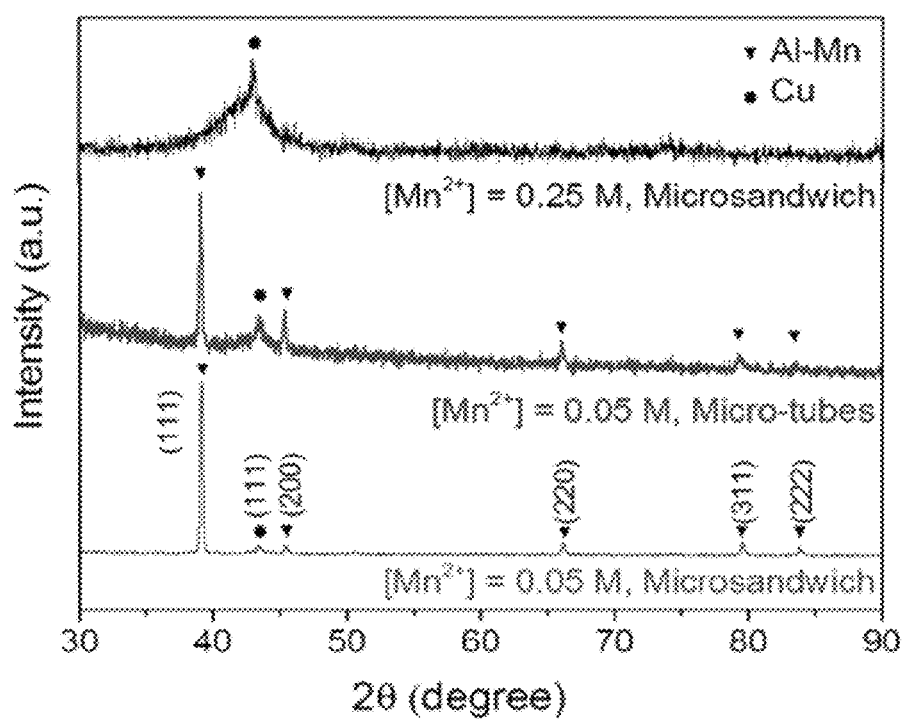


FIG. 4D

**FIG. 5**

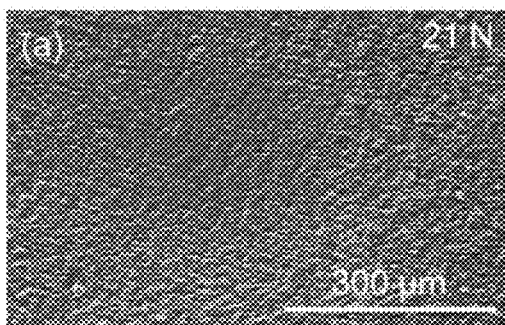


FIG. 6A

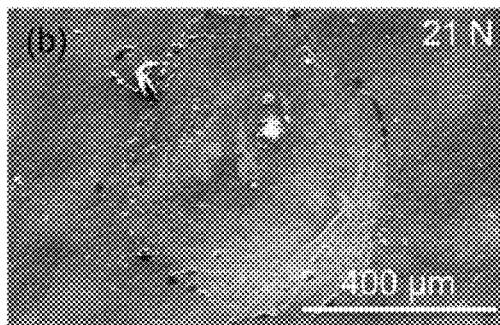


FIG. 6B

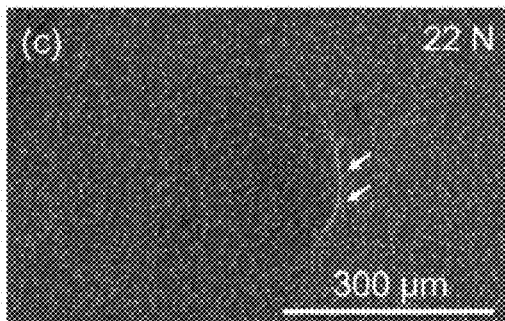


FIG. 6C

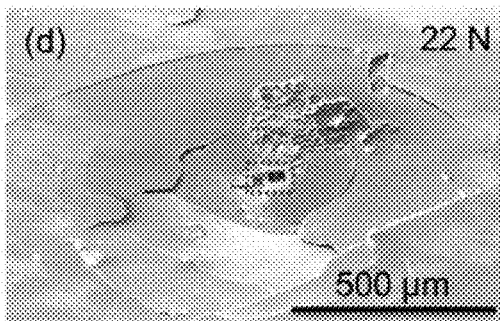


FIG. 6D

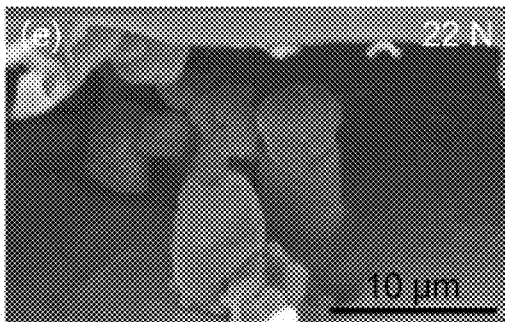


FIG. 6E

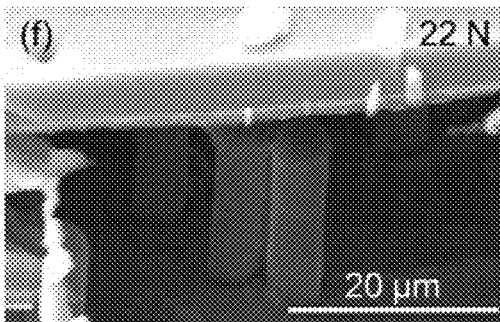


FIG. 6F

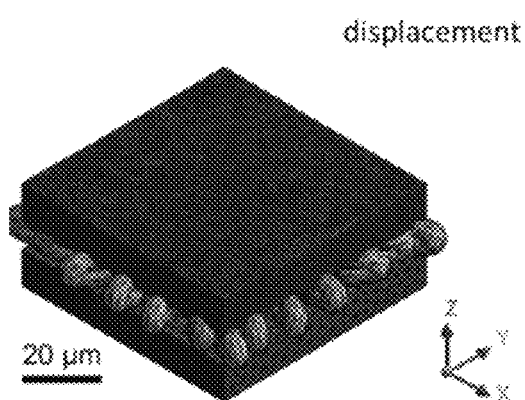


FIG. 7A

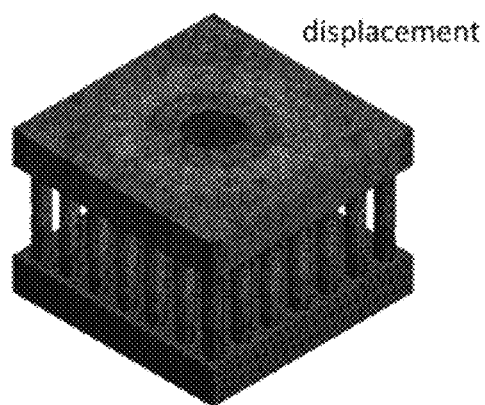


FIG. 7B

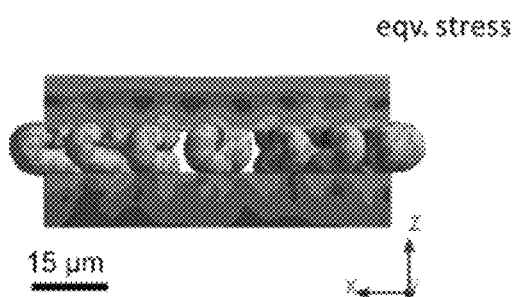


FIG. 7C

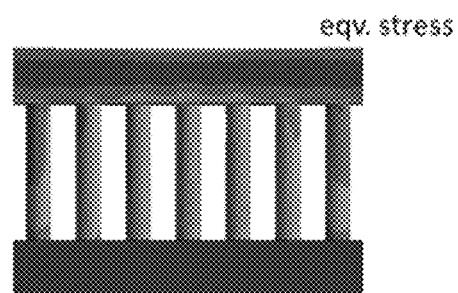


FIG. 7D

1

ELECTRODEPOSITION OF METAL
MICROSTRUCTURESCROSS-REFERENCE TO RELATED
APPLICATION

This application claims priority to U.S. Provisional Application Ser. No. 62/076,591, filed Nov. 7, 2014, which is hereby incorporated by reference herein in its entirety.

BACKGROUND

Micro-architected structures, or “microstructures,” including microlattices and microsandwiches, have recently emerged as promising structural and functional frameworks for small-scale multi-functional devices. The open architecture of such structures not only leads to low areal density and high damage tolerance, but also provides channels for heat and fluid flow, which are critical to multi-functional devices, such as high capacity batteries, insect-like robots, and micro-air vehicles. Sandwich structures, which comprise a core that extends between opposed end plates, exhibit higher bending rigidity than lattices by effectively redistributing the mass to the outer surfaces (instead of the core), similar to natural cellular materials found in insects and plants. Such superior properties have led to extensive studies on the structural performance of sandwich structures, mostly with physical dimensions above tens of centimeters. The damage tolerance of sandwich structures is highly dependent on the density, strength, and geometry of the core. It was found that a periodic sandwich core can be optimized to sustain loads at much lower relative densities than stochastic foams. Further improvement of mechanical properties may also be achieved by hybridizing the core material.

Existing fabrication procedures for large-scale sandwich structures typically involve welding or adhesive bonding of the face sheets and the core. These techniques become challenging as the size of the sandwich's core decreases to the nano- or micro-scale. Recently there have been several successful attempts to create microlattice and microsandwich structures from polymers, ceramics, and metals. Unfortunately, the fabrication processes used to construct these microstructures are complicated or limited to specific materials. It can therefore be appreciated that it would be desirable to have a more simple fabrication technique for such microstructures.

BRIEF DESCRIPTION OF THE DRAWINGS

The present disclosure may be better understood with reference to the following figures. Matching reference numerals designate corresponding parts throughout the figures, which are not necessarily drawn to scale.

FIGS. 1A-1D are sequential images illustrating steps of a first embodiment of a method for fabricating a microstructure.

FIGS. 2A-2D are sequential images illustrating steps of a second embodiment of a method for fabricating a microstructure.

FIG. 3 is a graph that plots cyclic voltammograms recorded in an AlCl_3 -EMIC electrolyte containing 0.5 and 0.25 M $[\text{Mn}^{2+}]$.

FIGS. 4A-4D are scanning electron microscope (SEM) images of a microsandwich structure (4A and 4B) and microtube structure (4C and 4D) electrodeposited using an AlCl_3 -EMIC electrolyte containing 0.5 $[\text{Mn}^{2+}]$.

2

FIG. 5 is a graph that plots x-ray diffraction (XRD) 2 θ scans of microtube and microsandwich structures.

FIGS. 6A-6F are SEM images of a surface (6A and 6B) and cross-section (6C and 6D) of Al-9 at. % Mn and Al-26 at. % Mn pillars after microindentation, and structural failure of the microsandwich structure (6E and 6F).

FIGS. 7A-7D are renderings of finite element analysis (FEA) predicted displacement (7A and 7B) and equivalent stress (7C and 7D) of Al-9 at. % Mn and Al-26 at. % Mn pillars after microindentation.

DETAILED DESCRIPTION

As described above, it would be desirable to have a simple fabrication technique for microstructures. Disclosed herein are example methods for fabricating microstructures, such as microsandwich structures. In some embodiments, a non-conductive polymer membrane comprising a plurality of elongated pores formed therein is coated with a conductive material, such as a metal, and a metal alloy, such as an aluminum (Al) alloy, is electrodeposited on the conductive material at room temperature in an ionic liquid electrolyte under galvanostatic control. In some embodiments, the composition (i.e., microstructure) of the alloy can be altered by changing the concentration of the alloyed metal present within the electrolyte.

In the following disclosure, various specific embodiments are described. It is to be understood that those embodiments are example implementations of the disclosed inventions and that alternative embodiments are possible. All such embodiments are intended to fall within the scope of this disclosure.

Disclosed in the following disclosure are methods for fabricating crystalline and amorphous alloy microstructures, such as microtube and microsandwich structures, using template electrodeposition. In some embodiments, the alloy comprises an alloy of Al and a transition metal that increases the strength of the metal. By way of example, the alloy can comprise an Al-manganese (Mn) alloy. The microstructures can be fabricated using a one-step electrodeposition process using a room temperature ionic liquid. The disclosed methods offer an opportunity to create Al alloy microstructures with low density, open architecture, and high specific strength and damage tolerance. Such microstructures can, for example, be used in applications as plasmonic pixels in color displays, anodes for lithium (Li) ion batteries, energy adsorbers, and the like.

FIG. 1 illustrates fabrication steps of an embodiment of a method for fabricating an alloy microstructure. More particularly, FIG. 1 illustrates a method for fabricating Al alloy microtube or microrod structure.

Beginning with FIG. 1A, a non-conductive polymer membrane 10 is formed that comprises a plurality of pores 12 that extend from a first or bottom end 14 of the membrane to a second or top end 16 of the membrane. In some embodiments, the membrane 10 is approximately 5 μm to 10 cm thick, in which case the pores 12 can also be approximately 5 μm to 10 cm long. In other embodiments, the thickness of the membrane 10 and the length of the pores 12 are approximately 10 to 30 μm . As shown in FIG. 1A, the pores 12 can be elongated, parallel, cylindrical pores that are arranged in an equally spaced, orthogonal grid pattern. In some embodiments, the pores 12 can have diameters of approximately 100 to 600 nm. It will be understood, however, that the pores 12 can have other configurations and dimensions, if desired. In some embodiments, the non-conductive polymer comprises polycarbonate. Polycarbon-

ate is a suitable material for this application because it can be easily removed after the desired Al alloy structures have been formed, as described below.

With reference to FIG. 1B, an end (the bottom end **14** in this example) of the membrane **10** is coated with a layer of conductive material so as to form a first or bottom layer **18** of conductive material. By way of example, the conductive material can be copper (Cu), which can be sputtered onto the membrane with a thickness of approximately 200 to 300 nm. Notably, the conductive material is deposited on not only the bottom end **14** of the membrane **10** but also on the inner surfaces of the pores **12** such that the Al alloy can be grown on both the bottom end and within the pores of the membrane.

Next, the Al alloy can be electrodeposited on the conductive material. In some embodiments, the Al alloy is deposited using a one-step, three-electrode galvanostatic electrodeposition process in which the coated membrane **10** acts as the cathode or working electrode in the process. The coated membrane **10** can be placed in a room temperature ionic liquid electrolyte that contains Al and the other metal to be deposited on the copper coating through electrodeposition. In some embodiments, the electrolyte comprises a solution of AlCl_3 , 1-ethyl-3-methyl-imidazolium chloride (EMIC), and MnCl_2 . As described below, the microstructure of the Al alloy to be formed can depend upon the concentration of the alloyed metal (e.g., Mn) within the electrolyte. In some embodiments, the Al alloy can have a crystalline microstructure. In other embodiments, the Al alloy can have an amorphous microstructure.

With reference next to FIG. 1C, as the Al alloy is deposited, it forms an end plate **20** at the bottom end **14** of the membrane **10** and fills the pores **12** of the membrane to create either microtubes or microrods. Whether microtubes or microrods are formed can depend upon various factors, such as the diameter of the pores **12**, the current density used during electrodeposition, and the duration of the electrodeposition. In some embodiments, the electrodeposition can be performed at a cathodic current density of approximately 6 mA/cm^2 for approximately 3 to 10 minutes.

Irrespective of whether microtubes or microrods are formed, the non-conductive polymer of the membrane **10** can next be removed, as indicated in FIG. 1D, so as to obtain free-standing microtubes or microrods **22** (microtubes shown in FIG. 1D). In some embodiments, the polymer can be removed by dissolving it using dichloromethane. Once the polymer is removed, a microstructure results that has a bottom plate **20** and multiple microtubes/microrods **22** having free ends extending therefrom.

FIG. 2 illustrates fabrication steps of an embodiment of a method for fabricating a further type of an alloy microstructure. More particularly, FIG. 2 illustrates a method for fabricating Al alloy microsandwich structures. As used herein, the term "microsandwich structure" refers to a structure in which a core comprising one or more hollow tubes or solid rods are terminated at their opposite ends by end plates.

The process used to fabricate a microsandwich structure is similar to the process described above in relation to FIG. 1. Accordingly, as shown in FIG. 2A, a non-conductive polymer membrane **10** is formed that comprises a plurality of pores **12** that extend from a first or bottom end **14** of the membrane to a second or top end **16** of the membrane. The membrane **10** and pores **12** can have configurations and dimensions similar to those of the like-named features described above.

With reference to FIG. 2B, the membrane **10** is coated with a layer of conductive material, such as Cu, so as to form

a first or bottom layer **18** and a second or top layer **24** of conductive material. As before, the conductive material is also deposited on the inner surfaces of the pores **12** such that the Al alloy can be grown on both the ends and within the pores of the membrane.

Next, referring to FIG. 2C, the Al alloy can be electrodeposited in similar manner to that described above in relation to FIG. 1. Through such electrodeposition, the Al alloy can form first and second, or bottom and top, end plates **26** and **28** over the bottom and top layers **18**, **24** of conductive material and fill the pores **12** of the membrane to form pillars of the microsandwich structure. Whether the pillars will comprise microtubes or microrods can depend upon various factors, such as the diameter of the pores, the current density used during electrodeposition, and the duration of the electrodeposition.

The non-conductive polymer of the membrane **10** can next be removed, as indicated in FIG. 2D, so as to form pillars **30** that extend between the end plates **26**, **28**. As shown in this figure, the pillars **30** can be equally spaced, cylindrical, and generally perpendicular to the bottom and top end plates **20**, **24**, which are generally parallel to each other. In some embodiments, the pillars **30** are hollow. In other embodiments, the pillars **30** are solid. Regardless, the pillars **30** are small in scale and, like the pores **12**, can be approximately 5 μm to 10 μm long. In some embodiments, the pillars **30** have a microscale and are approximately 10 to 30 μm long.

Structures of the types described above were fabricated using the above-described methods. Track-etched polycarbonate membranes (Cyclopre) having average nominal pore diameters of 5 μm were sputtered (CRC sputter coater, 99.99% argon (Ar), 5 mTorr) with a Cu layer of approximately 250 nm thickness on both sides of the membrane prior to electrodeposition. The electrodeposition was performed at room temperature using a three-electrode setup inside an Ar-filled glovebox (Mbraun Labstar, $\text{O}_2 < 1$ ppm, $\text{H}_2\text{O} < 1$ ppm). Al wire (99.99%, Alfa Aesar) was used as the reference electrode. The Cu-coated polycarbonate membranes (working electrodes) were placed in the middle of two parallel Al anodes (99.99%, Alfa Aesar), enabling Al—Mn to be deposited from both ends of the pores. The ionic liquid electrolyte was made by mixing AlCl_3 (anhydrous, 99.999%, Alfa Aesar) and EMIC (>98%, Iolitec) in 2:1 molar ratio. As-received EMIC was dried under vacuum at 60° C. for at least 24 hours prior to mixing. The electrolyte was then purified using Al plate under agitation until a vanish yellow color was achieved. MnCl_2 (98%, GFS Chemicals) was added to the electrolyte in different molarities and agitated for 24 hours. Galvanostatic electrodeposition was performed using Gamry Reference 600 potentiostat/galvanostat at 10 mA/cm^2 for 1 hour. Finally, free-standing microsandwich structures were obtained by dissolving the polycarbonate membrane using dichloromethane.

Cyclic voltammetry experiments were performed on a tungsten wire (~1 mm diameter) working electrode at a scan rate of 20 mV/s. The deposited structures were characterized using X-ray diffraction (XRD) (PANalytical X'Pert PRO), scanning electron microscopy (SEM) (Hitachi SU-70), and energy-dispersive X-ray spectroscopy (EDS) (EDAX-Phoenix). Cross-sections of the microsandwich structures were obtained by ion milling using focused ion beam microscopy (FIB) (FEI Quanta 200). Special care was taken to minimize gallium (Ga) contamination by using reduced current density during the final milling steps. Nanoindentation of the deposits was performed using a triboindenter (Hysitron,

Ti900) with a diamond Berkovich tip (~125 nm radius) at a 7 mN maximum load, a 1.4 mN/s loading/unloading rate, and a 2 second holding time. Microindentation (UMT-2, CETR) tests were performed using an alumina ball (4 mm diameter) tip under a constant normal load (varied from 20 to 25 N).

FIG. 3 shows the typical cyclic voltammograms recorded at the working electrodes in 66.7-33.3 mol % AlCl_3 -EMIC electrolyte containing 0.05 and 0.25 M $[\text{Mn}^{2+}]$. The scan started from 2 V versus Al/Al^{3+} and was reversed at -0.5 V versus Al/Al^{3+} . Mn is nobler than Al in aqueous solution, but in acidic chloroaluminate electrolyte (with a molar fraction of $\text{AlCl}_3 > 0.5$), the deposition potential for Mn is slightly more negative than that for Al. The forward scan in FIG. 3 is similar to that reported for pure Al and therefore shows no obvious reduction wave associated with $[\text{Mn}^{2+}]$. This indicates that Mn co-deposited with Al at potentials lower than approximately 0.1 V versus Al/Al^{3+} in the ionic liquid with 0.05 M $[\text{Mn}^{2+}]$. The overall reduction of Al—Mn occurred by the following reactions:



In the reverse scan, Al—Mn dissolution occurred at potentials higher than approximately 0.3 V versus Al/Al^{3+} . Increasing $[\text{Mn}^{2+}]$ in the electrolyte shifted the reduction potential in the anodic direction and the dissolution potential in the cathodic direction. In addition, the current densities decreased by approximately 40% as $[\text{Mn}^{2+}]$ increased from 0.05 to 0.25 M. This is similar to that reported by others, who found that the addition of $[\text{Mn}^{2+}]$ inhibits the nucleation of Al. EDS (EDAX-Phoenix) analysis showed that increasing $[\text{Mn}^{2+}]$ from 0.05 to 0.25 M increased the Mn concentration in the deposits from 9.0 ± 0.3 at. % to 26.2 ± 0.4 at. %. During co-deposition of Al and Mn, the alloy composition is mainly governed by the concentrations of the electroactive species Al_2Cl_7^- and Mn^{2+} . $[\text{Al}_2\text{Cl}_7^-]$ strongly depends on the acidity of the electrolyte. Under Lewis base conditions (molar fraction of $\text{AlCl}_3 < 0.5$), $[\text{Al}_2\text{Cl}_7^-]$ is close to zero ($< 10^{-7}$ M). Thus, maintaining a Lewis acid electrolyte is desirable for the deposition of an Al—Mn binary alloy. It should also be noted, however, that this condition is not necessary for Al—Mn deposition in inorganic chloroaluminate electrolyte systems in which the deposition can take place involving the discharge of Al_2Cl_4^- in basic solution.

Al—Mn microsandwich structures were successfully electrodeposited from acidic AlCl_3 -EMIC- MnCl_2 electrolyte contains 0.05 M $[\text{Mn}^{2+}]$ following the procedures described above in relation to FIG. 2. Galvanostatic control was chosen to better control the size of the deposited structures. FIG. 4A shows a SEM image of the microsandwich structure having approximately 11 μm thick end plates separated by 27.6 ± 0.6 μm tall pillars, which resembles the ancient Temple of Athena Nike. FIG. 4B shows a partial cross-section of the microsandwich structure. Both the Cu coating (light contrast) and the Al—Mn pillar (dark contrast) can be seen clearly in this figure. In this example, the pillars were formed as solid rods.

To evaluate the microsandwich growth kinetics, selected electrodeposition was carried out for 3 and 10 minutes using one Al plate as an anode. The deposited microstructures were free standing microtubes having various wall thicknesses. Typical SEM images of the microtubes are shown in FIGS. 3C and 3D. The microtubes were hollow and had an average height of 9.8 ± 0.9 μm . Increasing the deposition time from 3 to 10 min lead to thickening of the tube walls from 670 ± 100 nm to 1.2 ± 0.4 μm without affecting the tube length.

The inset in FIG. 4D shows a close-up of a microtube after 10 minutes of deposition. It can be seen that the deposition advanced in the radial direction of the pore and the inner microtube surface roughness increased with deposition time. During electrodeposition, kinetic roughening is often observed following a power law $\langle w \rangle \propto t^\beta$, where w represents the surface width, i.e., the average edge length projected on the substrate, and t is the deposition time. The power exponent β typically varies from 0.2 to 0.5, depending on deposition parameters such as the current density and electrolyte concentration. Measurements of the inner microtube surfaces indicate an approximate 36% increase of the surface width as the deposition time increased from 3 to 10 minutes, yielding a power exponent $\beta \approx 0.25$.

XRD results of the microtube and microsandwich structures are presented in FIG. 5. At 0.05 M $[\text{Mn}^{2+}]$, the XRD pattern of the microtube and microsandwich structures exhibited a single set of fcc peaks (lattice constant ≈ 4.00 Å) in addition to Cu (111), indicating the formation of a superaturated solid solution of Al—Mn. This Mn concentration (9.0 at. %) is significantly higher than the equilibrium solubility of Mn in Al at room temperature (≈ 0.62 at. %). For the microsandwich structure, a pronounced $\langle 111 \rangle$ fiber texture developed along the pillar direction, similar to that observed in other fcc metallic nanowires. At 0.25 M $[\text{Mn}^{2+}]$, the XRD pattern of the microsandwich structure indicates the formation of a complete amorphous phase (with possible local ordering), as represented by the diffuse peak at $2\theta \approx 42^\circ$. These results indicate that Mn, which has a Goldschmidt radius approximately 11% smaller than Al, is substitutionally incorporated into the Al lattice. Further increasing alloy content frustrates the ordered structure and leads to the formation of amorphous phase.

The hardness of the crystalline (Al-9 at. % Mn) and amorphous (Al-26 at. % Mn) deposits was 2.59 ± 0.21 GPa and 6.14 ± 0.35 GPa respectively, obtained using Oliver-Pharr method. Given the low density of Al alloys ($\rho_{\text{Al-9Mn}} \approx 3.12$ g/cm³ and $\rho_{\text{Al-26Mn}} \approx 3.94$ g/cm³) and the open architecture, the density of the microsandwich structures is estimated to be approximately 1.50 g/cm³ (relative density $p = 0.48$) and 1.89 g/cm³ (relative density $p = 0.48$) for the crystalline and amorphous structure respectively. The estimated specific strengths of the microsandwiches were between 277 and 520 kN·m/kg, which is well in excess of most commercial engineering alloys such as steel (130 kN·m/kg) and Ti-6Al-4V (240 kN·m/kg).

A preliminary study was performed to evaluate the impact damage resistance of the microsandwich structures under a 20 to 25 N normal load. It was observed that top plate cracks began to develop in the crystalline microsandwich at loads larger than approximately 22 N. On the other hand, large scale cracks were observed on the top plates of the amorphous microsandwich structures under all investigated loads. FIGS. 5A-D show typical SEM images of the surface of the microsandwich structures indented with forces of 21 and 22 N. The failure modes were similar to those reported for macroscale sandwich structures. The crystalline microsandwich structures mainly failed by pillar compression (see FIG. 6E) with minimal deformation of the top plate. The height of the deformed pillars beneath the indent was approximately 8.3 ± 0.5 μm , corresponding to a local compressive strain of approximately 70%. An arc-shaped crack was developed near the edge of the contact area under 22 N (see FIG. 6A), characteristic of ductile intergranular fracture. The failure mode of the amorphous microsandwich structure (see FIGS. 6B and 6D) was mainly the brittle

fracture and collapse of the top plate, while the pillars underneath retained their original shapes (see FIG. 6F). Debonding between the top plates and the cores was observed in both samples.

During indentation of a microsandwich structure, the core yield load (P_1) can be estimated as

$$P_1 = 1.52\sigma_c b t \left(\frac{E_c}{E_f} \frac{c}{t} \right)^{1/4} \quad (3)$$

where the core yield strength (σ_c , listed in Table 1) is calculated from nanoindentation hardness assuming a Tabor factor of three, the plate thickness t is 11 μm , the sample width b is 1 mm, the core thickness c is 27.6 μm , and the core-to-end plate elastic modulus ratio is approximately 1. The load for top plate fracture (P_2) and the plastic zone size (2s, as defined in FIG. 4) can be solved numerically from Equations (4) and (5):

$$\begin{aligned} & 2z^3(\sinh^2 z' + \sin^2 z') + \\ & \frac{3\lambda}{2\sigma_c b} P_2 = \frac{3(\sinh z' \cosh z' - \sin z' \cos z')(2z^2 - 1) - 6z}{z^2(\sinh^2 z' + \sin^2 z') +} \\ & 2z(\sinh z' \cosh z' - \sin z' \cos z') - (\cosh^2 z' + \cos^2 z') \end{aligned} \quad (4)$$

and

$$\left(\frac{\lambda}{\sigma_c b} \right) P_2 = \frac{\frac{\lambda^2 t_f^2 \sigma}{3\sigma_c} + z^2 + 2zA + B}{z + A} \quad (5)$$

Where

$$z = \lambda s, z' = \lambda s', \lambda = \left(\frac{3E_f}{E_c t} \right)^{1/4}, A = \frac{\sinh z' \cosh z' - \sin z' \cos z'}{\sinh^2 z' + \sin^2 z'}$$

and

$$B = \frac{\sinh^2 z' - \sin^2 z'}{\sinh^2 z' + \sin^2 z'}.$$

The calculated results are listed in Table 1. For the crystalline microsandwich structure, the predicted plate fracture load was 23.4 N, which is close to the crack initiation load measured experimentally (~22 N). This load was also larger than the core yield load (18.2 N). Thus, extensive core compression occurred prior to plate crack formation. In addition, the predicted plastic zone size (300 μm) agrees well with the experimentally measured fracture size (dashed arc in FIG. 6C). For the amorphous microsandwich structure, the predicted core yield load (43.1 N) was much higher than the applied loads. Thus, no core compression was expected in this case. On the other hand, the brittle fracture of the top plate, in spite of a high plate fracture load (55.6 N), was likely related to the near-zero tensile ductility of amorphous metals, which lacks sufficient intrinsic micro-mechanisms to mitigate high stress concentrations at crack tips.

TABLE 1

Micro-sandwich composition	Elastic modulus (GPa)	Poisson's ratio	Yield strength (MPa)	Plastic zone size (μm)	Core yield load (N)	Skin fracture load (N)
Al-9 at. % Mn	81.5	0.301	863	300	18.2	23.4
Al-26 at. % Mn	103	0.318	2,050	300	43.1	55.6

To gain a further understanding of the failure mechanism of the microsandwich structures, finite element analysis (FEA) was performed using Ansys Workbench over an area of 70×70 μm^2 with pillars separated 10 μm apart. The dimensions of the microsandwich structure were taken from experimental measurements. Both Al-9 at. % Mn and Al-26 at. % Mn were assumed to be elastic-perfectly plastic with material properties listed in Table 1. The microsandwich structures were loaded at 0.81 N and subsequently unloaded to reproduce the experimentally measured displacement. The FEA results are shown in FIGS. 7A-7D. Under the same load, the crystalline microsandwich structures were plastically deformed with large displacement (see FIG. 7A), while the amorphous microsandwich structure only experienced elastic deformation (mainly on top plate, as shown in FIG. 7B). In both cases, the maximum equivalent stress and the critical shear strains always appeared near the end plate-core interface, in agreement with the pillar delamination location observed experimentally. The absorption energy per unit volume of the crystalline microsandwich structure was estimated to be approximately 43.2 MJ/m³, which was much higher than that of conventional aluminum foams under similar strain (e.g., ~1-4 MJ/m³ for ALPORAS).

From the foregoing disclosure, it can be appreciated that the crystallinity of the electrodeposited Al—Mn alloys of a microstructure can be tuned by controlling [Mn²⁺] in the electrolyte. Microsandwich pillars were found to grow along the radial direction of the template pores with tunable wall thickness by the deposition time. Given the flexibility and scalability of the electrodeposition process, the methods described herein present an interesting future direction for designing ultra-lightweight energy adsorbers with open architecture, high strength, and high damage resistance.

The invention claimed is:

1. A method for fabricating a metal microstructure, the method comprising:

forming a non-conductive polymer membrane having a plurality of pores;
coating at least one end of the membrane and inner surfaces of the pores with a conductive material to form a conductive coating;
electrodepositing a metal on the conductive coating; and
dissolving the membrane to obtain a free-standing metal microstructure having a least one metal end plate and multiple elongated metal members extending therefrom.

2. The method of claim 1, wherein the elongated metal members comprise solid aluminum alloy rods or hollow aluminum alloy tubes having free ends.

3. The method of claim 1, wherein the free-standing metal microstructure comprises two opposed metal end plates and wherein the elongated metal members comprise pillars that extend between the end plates.

4. The method of claim 3, wherein the pillars are hollow.

5. The method of claim 3, wherein the pillars are solid.

6. The method of claim 1, wherein forming a non-conductive polymer membrane comprises forming a polycarbonate membrane.

7. The method of claim 1, wherein coating at least one end of the membrane comprises coating only one end of the membrane with the conductive material.

8. The method of claim 1, wherein coating at least one end of the membrane comprises coating top and bottom ends of the membrane. 5

9. The method of claim 1, wherein coating the membrane comprises coating the membrane with copper.

10. The method of claim 1, wherein electrodepositing a metal comprises electrodepositing an alloy of aluminum and a transition metal. 10

11. The method of claim 1, wherein electrodepositing a metal alloy comprises electrodepositing an alloy of aluminum and manganese.

12. The method of claim 1, wherein electrodepositing a metal comprises placing the membrane in an ionic liquid electrolyte that contains aluminum ions and other metal ions to be deposited so as to deposit an aluminum alloy. 15

13. The method of claim 12, further comprising controlling the microstructure of the aluminum alloy by controlling a concentration of an electroactive species in the electrolyte so as to tune the composition and microstructure of the aluminum alloy. 20

14. The method of claim 13, wherein the aluminum alloy has a crystalline microstructure. 25

15. The method of claim 13, wherein the aluminum alloy has an amorphous microstructure.

* * * * *